Three-Dimensional Versus Radiographic Measurements for Analyzing Extra-Articular Distal Radius Malunion

Lionel Athlani, Audrey Chenel, Philippe Berton, Romain Detammaecker, Gilles Dautel

Three-dimensional versus radiographic measurements for analyzing extra-articular distal radius malunion

Lionel Athlani[(1)] *, Audrey Chenel[(2)], Philippe Berton[(2)], Romain Detammaecker[(1)], Gilles Dautel[(1)].

[1] Department of Hand Surgery, Plastic and Reconstructive Surgery, Centre Chirurgical Emile Gallé, CHU de Nancy, 49 rue Hermite, 54000 Nancy, France

[2] Newclip Technics, PSI Radius, 45 Rue des Garottières, 44115 Haute-Goulaine, France.

Authors :

Lionel Athlani, M.D : lionel.athlani@gmail.com

Audrey Chenel, Ph.D : achenel@newcliptechnics.com

Philippe Berton : pberton@newcliptechnics.com

Romain Detammaecker, M.D : romain.detammaecker@hotmail.fr

Dautel Gilles, M.D Ph.D : gillesdautel@mac.com

* **Corresponding author:** Lionel Athlani
Phone number: + 33 6 67 68 79 57
Email: lionel.athlani@gmail.com

Short Title: 3D method for analyzing distal radius malunion.

Conflict of interest: Audrey Chenel and Philippe Berton declare a conflict of interest with Newclip technics®. The authors declared no potential conflicts of interest with respect to the research, authorship, and/or publication of this article.

Acknowledgements: The authors wish to thank Dr Joanne Archambault for English language editing assistance. The authors also acknowledge the contribution of Newclip Technics for assisting in the 3D modeling.

Funding statement: The authors received no financial support for the research, authorship, and/or publication of this article.

Informed consent: Each author certifies that informed consent for participation in the study was obtained.

Three-dimensional versus radiographic measurements for analyzing extra-articular distal radius malunion

ABSTRACT

Purpose – The purpose of this study was to compare the accuracy of evaluating the deformity in distal radius malunions using plain radiographic measurements versus a three-dimensional (3D) method involving 3D computer bone models.

Methods – Consecutive patients who had an extra-articular distal radius malunion were included. Standard radiographs and CT scans of both wrists were performed. Palmar tilt, radial tilt and ulnar variance were measured on radiographs. The CT scan data were sent to a workstation and 3D bone surface models of the radius were created. The 3D palmar tilt, 3D radial tilt, 3D ulnar variance and axial rotational deformity were calculated.

Results – Thirteen patients with a mean age of 40 years (22–57) were included. The three 3D values were positively correlated with their corresponding radiographic values. Nevertheless, the 3D palmar tilt and 3D radial tilt values were slightly smaller than the radiographic palmar tilt and radial tilt. The quantitative difference between the 3D method and plain radiographs was on average 2° for the dorsal deformity group and 3° for the palmar deformity group. The 3D ulnar variance was significantly higher than the radiographic ulnar variance by an average of +1.3 mm for malunions with dorsal tilt (p=0.002) and +0.6 mm for malunions with palmar tilt (p=0.007). The 3D method allowed us to measure the extent of the axial rotational deformity, which was 9° on average (range 2 to 21°).

Conclusion – Despite small differences, measurements made on plain radiographs and 3D computer bone models are both accurate for evaluating the deformity in extra-articular distal radius malunions. Our 3D method seems to provide a more accurate measurement of ulnar variance, particularly for dorsally angulated cases, and is helpful for measuring rotational malalignment.

.

Key words: 3D, Computer-assisted preoperative planning, Corrective osteotomy, Distal radius malunion

Clinical Relevance: This article provides a comprehensive set of distal radius measurements using a 3D computer bone model and plain radiographs. In this study, we found that both methods can be used as a benchmark for evaluating the deformity of extra-articular distal radius malunion. The 3D method can also be used to define the axial rotational deformity.

INTRODUCTION

Patients with symptomatic distal radius malunion are candidates for corrective osteotomy surgery. The deformity is typically evaluated using plain radiographs (1-3) and the differences in palmar tilt, radial tilt, and ulnar variance between the normal and affected sides have been used to determine the amount of deformity correction required (4-6). However, distal radius malunion is considered a three-dimensional (3D) deformity and pre-operative planning based on plain radiographs may not be sufficiently accurate to ensure anatomical correction (7-10). Prommersberger et al. (3) and Von Campe et al. (6) have shown that residual deformity is present in more than 50% of cases and that it negatively affects the functional outcome . Recently, 3D bone models created from computed tomography (CT) data have been used to quantify the deformity (11, 12). Using 3D models, Gray et al. (4) found that the contralateral radius can be used to define normal anatomy and serve as a reference during preoperative planning for malunion surgery. In a multicenter study, Buijze et al. (13) compared the results of corrective osteotomy for extra-articular distal radial malunion performed with 3D versus two-dimensional (2D) preoperative planning. They found no clinical differences between the two groups of patients. Nevertheless, radiographic analysis showed significant differences in the average residual palmar tilt and radial tilt compared with the healthy contralateral side, in favor of 3D method. The purpose of this study was to compare the accuracy of evaluating the deformity in distal radius malunions using plain radiographic measurements versus a three-dimensional (3D) method involving 3D computer bone models.

METHODS

Study population

Between December 2016 and March 2019, consecutive patients who had an extra-articular distal radius malunion were included after they provided informed consent and institutional review board approval was obtained. Initially, all patients had sustained an extra-articular fracture treated by cast immobilization. These patients had been referred to us because of wrist

pain, deformity, and/or limited pronation–supination. They had not previously undergone surgery. Standard (posteroanterior and lateral) radiographs and low-dose CT scans (Aquilion ONE; Canon Medical Systems, Otawara, Japan) of both wrists including the forearms were made for each patient.

Radiographic evaluation

Palmar tilt (accuracy of 1°), radial tilt (accuracy of 1°), and ulnar variance (accuracy of 0.1 mm) were measured (Figure 1) by a single independent examiner (senior surgeon). The "normal" status of the contralateral wrist was always confirmed. Digital images were viewed on OsiriX© (Pixmeo® 2016, Geneva, Switzerland).

3D evaluation

The CT scan data were sent to a workstation in standard DICOM format. The 3D bone surface models of the radius were created using Simpleware software (Synopsys Inc, Mountain View, CA, USA) provided by **Blinded by JHS** . The locations of the relevant points and axes were determined on the 3D bone surface models by a single engineer specialized in biomechanics who was blinded to the radiography findings. For the affected and contralateral wrists, the 3D palmar tilt (accuracy of 1°), 3D radial tilt (accuracy of 1°) and 3D ulnar variance (accuracy of 0.1 mm) were calculated based on these points using computer-aided design software (3D Creo Parametric®, PTC, Boston, USA) (Figure 2). The radial styloid and midway points were defined to minimize the impact of the sagittal plane deformity when calculating 3D radial tilt and 3D ulnar variance.

The amount of deformity was defined for the three 3D measurements as the difference between the two sides in the coronal and sagittal planes. The axial rotational deformity was analyzed by superimposing the 3D image of the affected radius onto the 3D mirror image of the contralateral normal radius. Then, we evaluated the magnitude of the axial rotational deformity by calculating

the difference—in degrees (accuracy of 1°)—between the two axial planes defined for the two images superimposed proximally to distally (Figure 3).

Statistical analysis

For the two subgroups, the mean values and ranges were calculated. Differences between the radiographic and 3D methods were assessed using Student's *t*-test. Correlations between two continuous variables were investigated using Pearson's correlation coefficient (*r*) and simple regression analysis. Data were deemed significant if *p* values were less than 0.05.

RESULTS

Patients

Thirteen patients (5 men, 8 women) with a mean age of 40 years (22–57) were included. The dominant upper limb was involved in 5 cases. The average interval between the fracture event and our examination was 5 months (range 3–10). The 13 patients were divided into two sub-groups based on their sagittal deformity: dorsal deformity type (malunion with dorsal tilt, n=7) or palmar deformity type (malunion with palmar tilt, n=6). The results for each patient are presented in Table 1.

Palmar tilt comparison

In the dorsal deformity group, the average palmar tilt on plain radiographs of the affected wrists was −19° (range −5° to −42°), whereas that of the contralateral normal wrist was +8° (range +5° to +12°). On the 3D models, the average 3D palmar tilt was −18° (range −2° to −39°) and +8° (range +4° to +12°), respectively.

In the palmar deformity group, the average palmar tilt on plain radiographs of the affected wrists was +29° (range +16° to +39°), whereas that of the contralateral normal wrist was +9° (range +5° to +11°). On the 3D models, the average 3D palmar tilt was +27° (range +19° to +37°) and +8° (range +4° to +12°), respectively.

In the both groups, the 3D palmar tilt was positively correlated with the radiographic palmar tilt (dorsal deformity group: $r = 0.98$, $p = 0.59$; palmar deformity group: $r = 0.95$, $p = 0.19$). The 3D palmar tilt had a smaller value than the radiographic palmar tilt (dorsal deformity group: $y = 0.9498x + 0.4$; palmar deformity group: $y = 0.811x – 3.8$). The quantitative difference between the 3D method and plain radiographs was on average 2° for the dorsal deformity group and 3° for the palmar deformity group.).

Radial tilt comparison

In the dorsal deformity group, the average radial tilt on plain radiographs of the affected wrists was 13° (range 5° to 15°), whereas that of the contralateral normal wrist was 23° (range 18° to 26°). On the 3D models, the average 3D radial tilt was 12° (range 2° to 19°) and 22° (range 18° to 25°), respectively.

In the palmar deformity group, the average radial tilt on plain radiographs of the affected wrists was 21° (range 14° to 29°), whereas that of the contralateral normal wrist was 22° (range 18° to 25°). On the 3D models, the average 3D radial tilt was 19° (range 10° to 26°) and 22° (range 19° to 26°), respectively.

The 3D radial tilt was positively correlated with the radiographic radial tilt (dorsal deformity group: $r = 0.84$, $p = 0.42$; palmar deformity group: $r = 0.91$, $p = 0.12$). However, the quantitative difference between the 3D method and plain radiographs was 3° on average for both groups.

Ulnar variance comparison

In the dorsal deformity group, the average ulnar variance on plain radiographs of the affected wrists was +1.9 mm (range −1.5 to +4 mm), whereas that of the contralateral normal wrist was −0.7 mm (range −2 to 0 mm). On the 3D models, the average 3D ulnar variance was +3.2 mm (range −0.7 to 5.5 mm) and −0.5 mm (range −2 to 0mm), respectively.

In the palmar deformity group, the average ulnar variance on plain radiographs of the affected wrists was +1.3 mm (range −1 to 3 mm), whereas that of the contralateral normal wrist was

−1.2 mm (range −2 to +0 mm). On the 3D models, the average ulnar variance was +1.9 mm (range −0.1 to 4.2 mm) and −1.1 mm (range −2 to 0 mm), respectively.

The 3D ulnar variance was positively correlated with the values on radiographs (dorsal deformity group: $r = 0.98$, $p = 0.002$; palmar deformity group: $r = 0.97$, $p = 0.007$). Both groups had a significant difference in the average 3D and radiographic ulnar variance with the 3D measurements being consistently higher . The difference was on average +1.3 mm for the dorsal deformity group ($p = 0.002$) and +0.6 mm for the palmar deformity group ($p = 0.007$).

Axial rotational deformity

The average axial rotational deformity was 9° (range 2 to 21°). It was 5° (range 2 to 12°) in the dorsal deformity group and 13° (range 2 to 21°) in the palmar deformity group.

DISCUSSION

The current study shows that the three 3D parameters describing the deformity in extra-articular distal radius malunions are positively correlated with those measured on radiographs. Moreover, we found that, in most cases, the values of palmar tilt, radial tilt and ulnar variance derived from 3D bone models differed only slightly from those derived from radiographs. However, on average, the 3D palmar tilt and 3D radial tilt were smaller than in the radiographic evaluation. Conversely, the 3D ulnar variance values were larger..

According to Von Campe A et al. (6), after corrective osteotomy using preoperative planning with plain radiographs, a residual deformity of more 10° with under-correction of the palmar tilt and overcorrection of the radial tilt deformity is often found. This may be the result of inadequate pre-operative analysis of those two values. On radiographs, the distal radius is seen in a 2D projected view. As the distal radius tilts more dorsally or more ventrally, the radial margin of the distal radial articular surface moves more proximally or more distally, and the angle changes (14). Therefore, one of the potential advantages of virtual preoperative planning

would be the possibility of simulating the change in radial tilt after the dorsal or palmar tilt deformity has been corrected. .

Ulnar variance is an important parameter for assessing shortening (3, 6). Therefore, we used the ulnar margin of the volar rim of the radial articular surface as a measuring point for ulnar variance on the radiographic evaluations. This point is not usable in 3D models because the sagittal deformity of the distal radius causes a measurement error. As a result, we used a point midway between the volar and dorsal rims of the ulnar margin of the radial articular surface as a reference point. In our study, ulnar variance was the only parameter with a significant difference between the 3D and 2D analysis. The 3D method found higher values while remaining quantitatively slightly different from those of the radiographic evaluation. This difference could be explained by the use of a "midway" point on 3D models. However, the use of the ulnar margin of the volar rim of the radial articular surface on radiographs could underestimate the magnitude of the shortening deformity, especially in cases of severe sagittal deformity. Von Campe et al. (6) noted that more 40% of patients had a residual shortening deformity of ≥ 1 mm after a surgical procedure in which the pre-operative planning was done with radiographs. Ulnar variance improves spontaneously after the sagittal and coronal plane deformities are corrected, without lengthening (15). Thereby, 3D analysis could be helpful for evaluating the relationship between the correction of palmar tilt, radial tilt and ulnar variance..

Since the axial rotational deformity cannot be detected radiographically, its extent cannot be quantified. We believe our 3D method allows the axial rotational deformity to be evaluated relative to the contralateral normal radius, which is the rotation reference for a given patient. However, in this study, we could not conclude that the axial rotational deformity is correlated with the differences between the radiographic and 3D evaluations. Lee et al. (16) found this deformity probably does not affect the radiographic parameters (palmar tilt, radial tilt and ulnar variance). For Shintani et al. (17), 3D deformity of the distal radius must include rotation deformity; 3D computer bone models could be used to assess it.

The generalizability of our results is limited since the size of study sample is small (n = 13). Nevertheless, according to our findings, measurements based on plain radiographs and 3D computer bone models are both accurate for evaluating the deformity of extra-articular distal radius malunion. Although the differences are small and possibly within the margin of error of what current surgical techniques can achieve, our 3D method seems to provide us with a more accurate measurement of ulnar variance, particularly for dorsally angulated cases, and is helpful for measuring rotational malalignment..

.

REFERENCES

1. Fernandez DL. Correction of post-traumatic wrist deformity in adults by osteotomy, bone-grafting, and internal fixation. *J Bone Joint Surg Am*. 1982; 64: 1164–1178.

2. Kreder HJ, Hanel DP, McKee M, Jupiter J, McGillivary G, Swiontkowski MF. X-ray film measurements for healed distal radius fractures. *J Hand Surg Am*. 1996; 21: 31–39.

3. Prommersberger KJ, Van Schoonhoven J, Lanz UB. Outcome after corrective osteotomy for malunited fractures of the distal end of the radius. *J Hand Surg Br*. 2002; 27: 55–60.

4. Gray RJ, Thom M, Riddle M, Suh N, Burkhart T, Lalone E. Image-Based Comparison Between the Bilateral Symmetry of the Distal Radii Through Established Measures. *J Hand Surg Am*. 2019; 44:966-972.

5. Hollevoet N, Van Maele G, Van Seymortier P, Verdonk R. Comparison of palmar tilt, radial inclination and ulnar variance in left and right wrists. *J Hand Surg Br.* 2000; 25: 431–433.

6. Von Campe A, Nagy L, Arbab D, Dumont CE. Corrective osteotomies in malunions of the distal radius: do we get what we planned? *Clin Orthop Relat Res*. 2006; 450: 179–185.

7. Athwal GS, Ellis RE, Small CF, Pichora DR. Computer-assisted distal radius osteotomy. *J Hand Surg Am*. 2003; 28: 951–958.

8. Bilic R, Zdravkovic V, Boljevic Z. Osteotomy for deformity of the radius. Computer-assisted three-dimensional modelling. *J Bone Joint Surg Br*. 1994; 76: 150–154.

9. Jupiter JB, Ruder J, Roth DA. Computer-generated bone models in the planning of osteotomy of multidirectional distal radius malunions. *J Hand Surg Am*. 1992; 17: 406–415.

10. Miyake J, Murase T, Yamanaka Y, Moritomo H, Sugamoto K, Yoshikawa H. Three-dimensional deformity analysis of malunited distal radius fractures and their influence on wrist and forearm motion. *J Hand Surg Eur*. 2012; 37:506-512.

11. Oka K, Murase T, Moritomo H, Goto A, Sugamoto K, Yoshikawa H. Corrective osteotomy using customized hydroxyapatite implants prepared by preoperative computer simulation. *Int J Med Robot*. 2010; 6: 186–193.

12. Miyake J, Murase T, Yamanaka Y, Moritomo H, Sugamoto K, Yoshikawa H. Comparison of three dimensional and radiographic measurements in the analysis of distal radius malunion. *J Hand Surg Eur Vol.* 2013; 38:133–143.

13. Buijze GA, Leong NL, Stockmans F, Axelsson P, Moreno R, Ibsen Sörensen A, Jupiter JB. Three-Dimensional Compared with Two-Dimensional Preoperative Planning of Corrective Osteotomy

for Extra-Articular Distal Radial Malunion: A Multicenter Randomized Controlled Trial. *J Bone Joint Surg Am*. 2018; 100:1191-1202.

14. Walenkamp MM, de Muinck Keizer RJ, Dobbe JG, Streekstra GJ, Goslings JC, Kloen P, Strackee SD, Schep NW. Computer-assisted 3D planned corrective osteotomies in eight malunited radius fractures. *Strategies Trauma Limb Reconstr*. 2015; 10:109-116.

15. Del Piñal F, Garcia-Bernal FJ, Studer A, Regalado J, Ayala H, Cagigal L. Sagittal rotational malunions of the distal radius: the role of pure derotational osteotomy. *J Hand Surg Eur*. 2009; 34: 160–165.

16. Lee SK, Shin R, Zingman A, Loona J, Posner MA. Correlation of malrotation deformity in distal radius fractures with radiographic analysis: cadaveric study. *J Hand Surg Am.* 2010; 35: 228–232.

17.Shintani K, Kazuki K, Yoneda M, Uemura T, Okada M, Takamatsu K, Nakamura H. Computer-Assisted Three-Dimensional Corrective Osteotomy for Malunited Fractures of the Distal Radius Using Prefabricated Bone Graft Substitute. *J Hand Surg Asian Pac Vol*. 2018; 23:479-486.

FIGURE LEGENDS

Figure 1. Measurement of palmar tilt, radial tilt, and ulnar variance on radiographs. Palmar tilt (A) was measured as the angle made by two lines on the lateral radiograph. A line perpendicular to the central long axis of the radius and a line between the dorsal and palmar margins of the distal radial articular surface. Radial tilt (B) was measured as the angle made by two lines on the posteroanterior radiographs. A line perpendicular to the central long axis of the radius and a line connected the radial styloid and ulnar margin of the distal radial articular surface. Ulnar variance (C) was measured as the distance between two lines perpendicular to the central long axis of the radius. The first line was at the ulnar margin of the distal radial articular surface and the second line was at the distal ulnar articular surface.

Figure 2. Deformity evaluation using 3D computer bone models. 3D palmar tilt (A) corresponds to the angle defined by a line perpendicular to the central long axis of the radius and a line passing through the palmar ulnar margin point and the dorsal ulnar margin point. 3D radial tilt (B) corresponds to the angle defined by a line perpendicular to the central long axis of the radius and the line passing through the radial styloid point and the midway point. 3D ulnar variance (C) corresponds to the distance between the line perpendicular to the central long axis of the radius and tangent to the distal end of the ulnar head then a line perpendicular to the radial shaft and passing through the midway point.
MP: midway point, RSP: radial styloid point, DUMP: dorsal ulnar margin point, PUMP: palmar ulnar margin point

Figure 3. Evaluation of axial rotational deformity using 3D computer bone models. Frontal planes for the contralateral normal radius (A) and the affected radius (B) pass proximally through the center of the radial head and radial diaphysis, and distally through the radial styloid point and the midway point. The axial rotational deformity was analyzed by superimposing the

3D image of affected radius onto a 3D mirror image of the contralateral normal radius (C). The magnitude of the deformity was evaluated by calculating the difference, in degrees, between the two axial planes defined for the two images superimposed proximally to distally (D). MP: midway point, RSP: radial styloid point

TABLE LEGENDS

Table 1. Radiographic and 3D measurements of palmar tilt, radial tilt and ulnar variance for each patient.

Figure 1

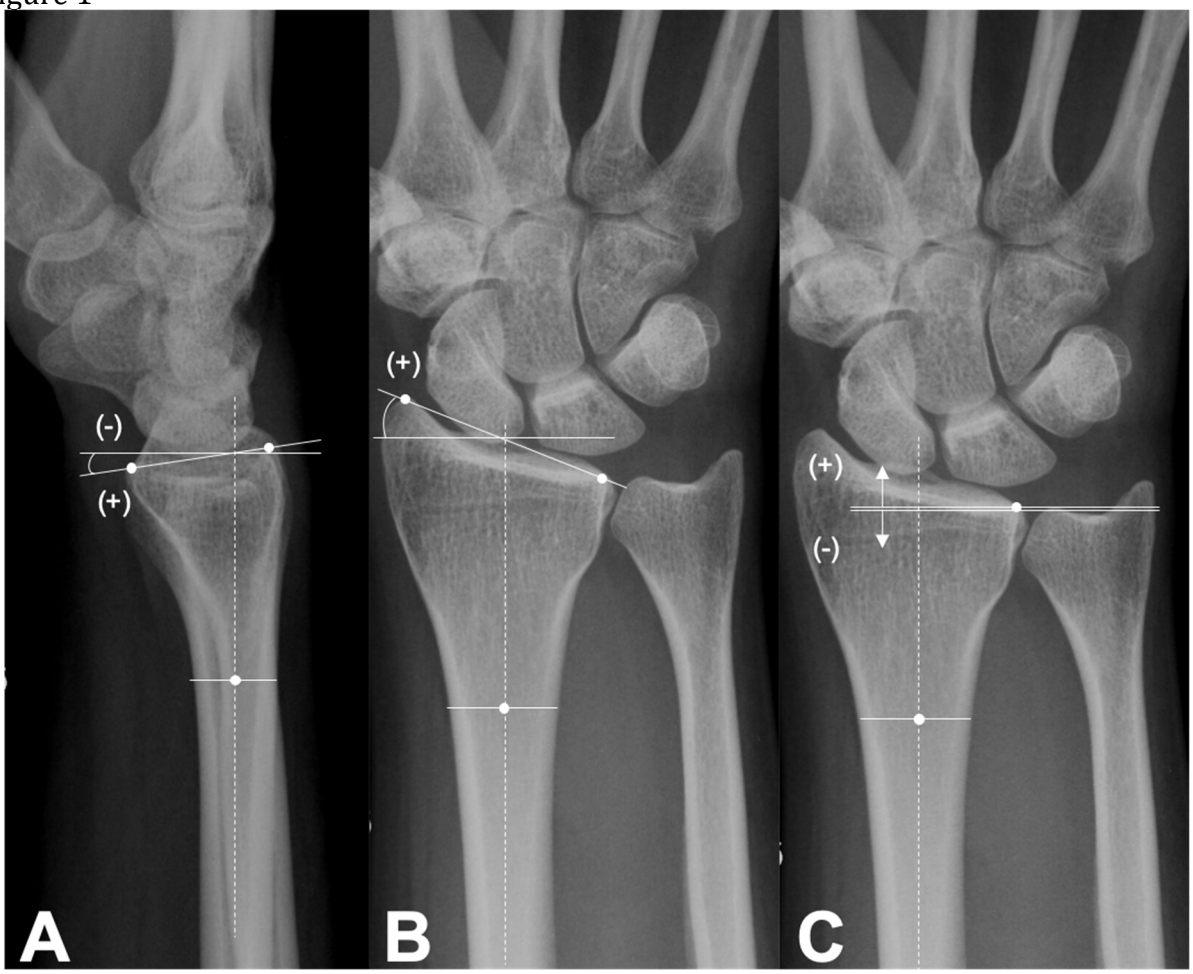

Figure 2

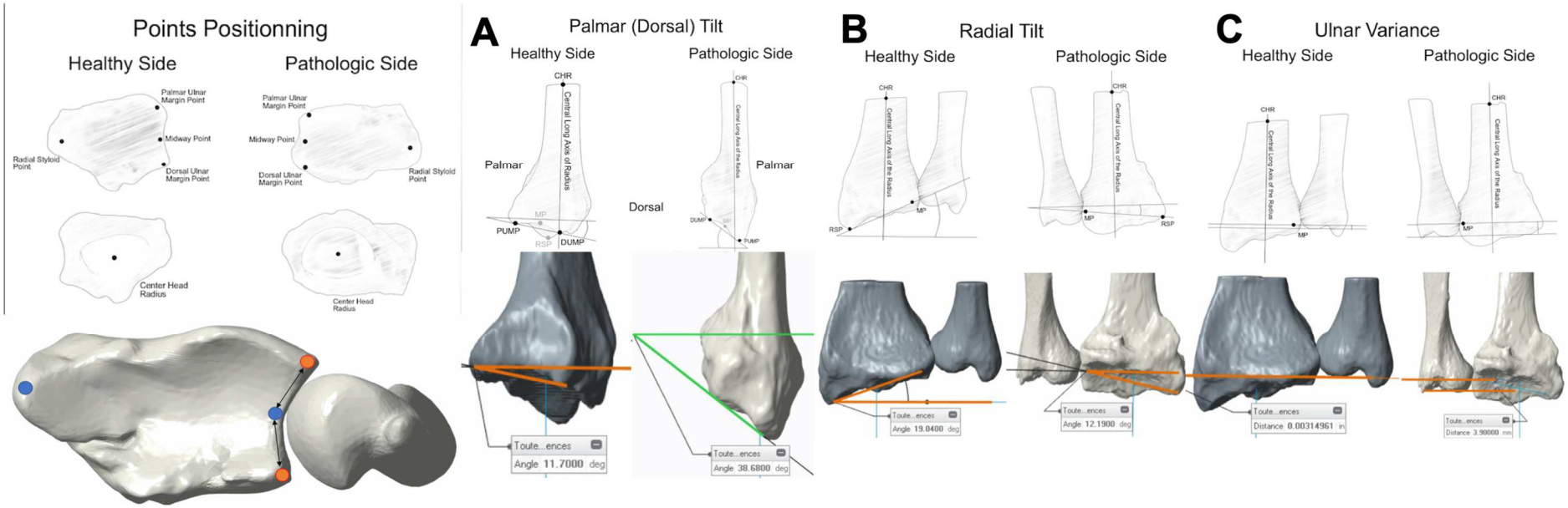
Points Positionning
Healthy Side
Pathologic Side
Palmar Ulnar Margin Point
Midway Point
Radial Styloid Point
Dorsal Ulnar Margin Point
Center Head Radius
A
Palmar (Dorsal) Tilt
Healthy Side
Pathologic Side
CHR
Central Long Axis of Radius
Palmar
Dorsal
MP
PUMP
RSP
DUMP
Toute...ences
Angle 11.7000 deg
Angle 38.6800 deg
B
Radial Tilt
Healthy Side
Pathologic Side
Angle 19.0400 deg
Angle 12.1900 deg
C
Ulnar Variance
Healthy Side
Pathologic Side
Distance 0.00314961 in
Distance 3.90000 mm

Figure 3

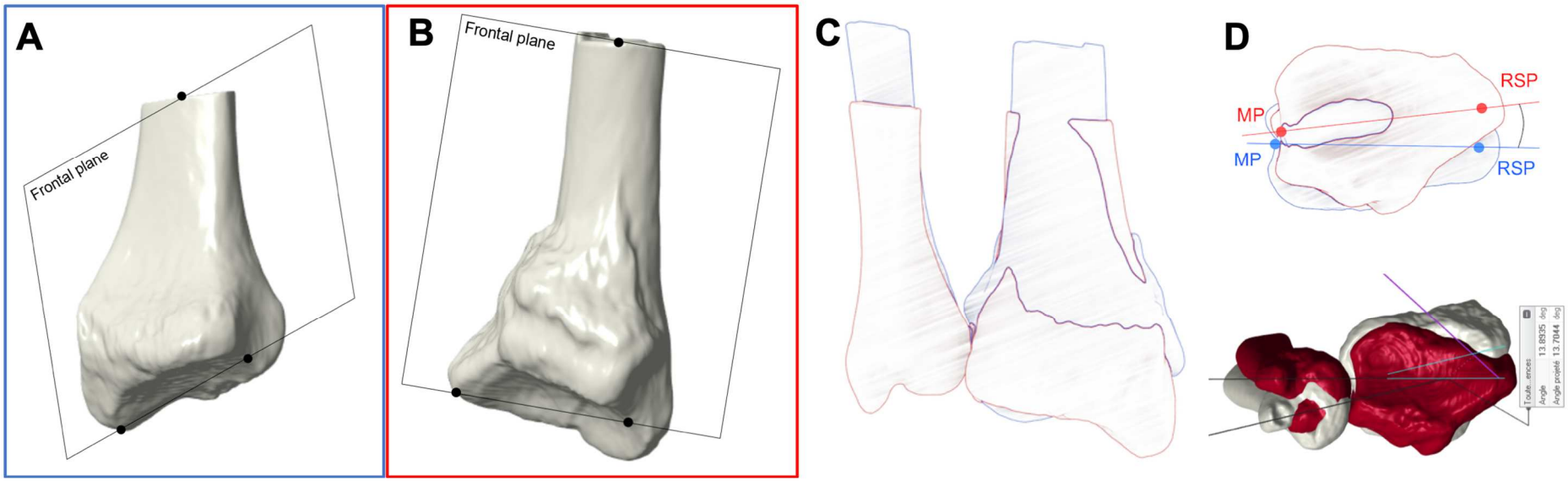

Table 1. Radiographic and 3D measurements of palmar tilt, radial tilt and ulnar variance for each patient.

Patient	Affected wrist	Palmar tilt (°)			Radial tilt (°)			Ulnar variance (mm)			Axial rotational deformity (°)
		Radiographic	3D	Difference	Radiographic	3D	Difference	Radiographic	3D	Difference	3D
Dorsal deformity group (n = 7)											
1	L	-28	-30	2	19	12	7	3.5	4.4	0.9	–
2	L	-10	-9	1	12	9	3	-1.5	-0.7	0.8	2
3	R	-5	-2	3	14	14	0	4	5.5	1.5	–
4	R	-14	-13	1	14	12	2	3	5.5	2.5	5
5	L	-42	-39	3	5	2	3	1	2.4	1.4	5
6	L	-11	-15	4	15	16	1	3.5	4.8	1.3	12
7	R	-21	-19	2	15	19	4	0	0.6	0.6	3
Average		-19	-18	2	13	12	3	1.9	3.2	1.3	5

Palmar deformity group (n = 6)											
1	L	+39	+37	2	16	10	6	3	4.2	1.2	2
2	R	+36	+32	4	29	26	3	1	1.4	0.4	20
3	L	+28	+23	5	21	22	1	1	1.3	0.3	15
4	L	+25	+23	2	14	13	1	-1	-0.1	0.9	21
5	R	+30	+30	0	23	18	5	2	2.4	0.4	15
6	L	+16	+19	3	25	26	1	1.5	2.1	0.6	4
Average		+29	+27	3	21	19	3	1.3	1.9	0.6	13

R: right; L: left.